Pergamon

Int. J. Solids Structures Vol. 33, No. 11, pp. 1563–1573, 1996

0020-7683/96 $15.00 + .00

0020-7683(95)00111-5

SINGULARITIES OF AN INTERFACE CRACK IMPINGING ON A TRIPLE GRAIN JUNCTION

CATALIN R. PICU
Thayer School of Engineering, Dartmouth College, Hanover NH 03755, U.S.A.

(*Received* 15 *January* 1995; *in revised form* 19 *April* 1995)

Abstract—The crack-tip stress-field singularity of a crack lying along a grain boundary and impinging on a grain triple junction is investigated. The three grains forming the triple junction are considered to be made from the same anisotropic material, albeit with different orientations of the principal material axes. The analysis is limited to elastic plane-strain deformation and is carried out using the Eshelby–Stroh formalism for anisotropic elasticity. The effect of the anisotropy on the level of the singularity is investigated for both transversely cubic and orthotropic grains.

1. INTRODUCTION

The problem of a crack between two isotropic or anisotropic materials has received much attention in the last decades due to its applications in decohesion and delamination problems. For a crack along an interface formed by two dissimilar isotropic materials, it was established (Williams, 1959) that close to the crack tip the stress field is singular and the singularity is complex. Similar to the standard solution for a crack in an homogeneous material, the real part of the singularity is $-\frac{1}{2}$ while the imaginary part is a function of the elastic constants of the two materials forming the interface. The complex singularity suggests an oscillatory behavior of the stress and displacement fields close to the crack tip involving the interpenetration of the crack faces. In a solution of the interface crack problem given by Comninou (1977a,b), this anomalous behavior is eliminated by considering the crack faces to be in contact close to the tip. The stress field of the corrected solution is singular with a $-\frac{1}{2}$ singularity and reduces to the previous solution by Williams outside a near-tip region.

Similar complex singularities of the stress field have been found for a crack between two anisotropic materials. The real part is still $-\frac{1}{2}$ while the imaginary part is a function of the elastic constants of the two materials forming the interface and the relative orientation of their principal axes of anisotropy (Ting, 1986). The conditions for the complex part to be zero and for the fields to be non-oscillatory were determined in a general form by Qu and Bassani (1989). When the two crystals forming the interface are made from the same material and if the out-of-plane deformation is decoupled from the in-plane one, which is the case for transversely orthotropic and cubic materials, the fields turn out to be non-oscillatory for any relative orientation of the principal material axes.

The stress concentration at grain triple junctions due to thermal expansion or elastic anisotropy is considered to be the principal mechanism responsible for crack nucleation in brittle materials at low temperatures and high strain rates. However, compared with the interface crack problem, the investigation of these concentration sites has received less attention. A weak logarithmic singularity was found by Evans (1978) and Fu and Evans (1985) to occur at a triple junction due to the thermal expansion anisotropy of the grains. The combined case when both thermal and elastic anisotropies are considered, was analyzed by Tvergaard and Hutchinson (1988). Their study is limited to planar triple junction geometries with symmetrical oriented grain boundaries 120° apart, and with one symmetric orientation of the material axes of the grains. The stress field was found to be singular with a leading real singularity ranging from -0.1 to -0.2 for typical engineering ceramics with cubic and orthotropic grains. Their study was extended by Picu and Gupta (1995) by considering a wide range of planar grain triple junction geometries. It was found that

symmetric configurations always lead to higher singularities. In Picu and Gupta (1995), complex values for the singularity exponent were found for several grain triple-junction geometries.

The combined case of a crack along an interface and impinging on a point of discontinuity such as a triple junction, has been rarely addressed. Chen and Hasebe (1993) considered the case of a crack along a wedge-shaped interface. The wedges, made from isotropic materials, are bounded along an interface and debonded along the other edge. Their results indicate a significant dependence of the leading eigenvalue on the material constants and the wedge angle. The real part of the singularity at the crack tip ranges from -0.35 to -0.65 when the wedge angle changes from 0° to 360°.

In this paper, the effect of the anisotropy on the stress-field singularity at the tip of a crack along a grain boundary and impinging on a triple grain junction is investigated. The three grains forming the triple junction are considered to be made from the same transversely orthotropic or cubic material and to have different orientations of the principal axes of anisotropy. The analysis is performed using the Eshelby–Stroh formalism for anisotropic elasticity. Since in the previous studies (Tvergaard and Hutchinson, 1988; Picu and Gupta, 1995) the symmetric configurations were found to lead to the most critical conditions, only such geometries are considered here. However, several non-symmetric cases have been investigated and the results support the choice. The results of the present study are significant for crack propagation problems in brittle materials such as ceramics or rock.

2. ESHELBY–STROH FORMALISM FOR ANISOTROPIC ELASTICITY

The constitutive law for a hyperelastic material within the small strain and rotation idealization can be written as

$$\sigma_{ij} = c_{ijks} u_{k,s}, \tag{1}$$

where c_{ijks} is the elasticity tensor relating the stresses σ_{ij} to the gradients of the displacement components u_k. For plane deformations with displacement field only a function of x_1 and x_2 (plane strain included), the displacement components u_k can be expressed in terms of an analytical function $f(Z)$ as (Eshelby *et al.*, 1953; Lekhnitskii, 1963)

$$u_k = \mathrm{a}_k f(Z), \quad k = 1, 2, 3 \tag{2}$$

with

$$Z = x_1 + p x_2.$$

Substituting eqn (2) in eqn (1) and using the equilibrium equations $\sigma_{ij,j} = 0$ leads to the following eigenvalue problem with eigenvalues p and eigenvector $\mathbf{a}$:

$$[c_{i1k1} + p(c_{i1k2} + c_{i2k1}) + p^2 c_{i2k2}]\mathrm{a}_k = 0. \tag{3}$$

Equation (3) can be expressed in matrix notation (Ting, 1986) by defining matrices $\mathbf{Q}$, $\mathbf{R}$ and $\mathbf{T}$ with components

$$Q_{ik} = c_{i1k1}, \quad R_{ik} = c_{i1k2}, \quad T_{ik} = c_{i2k2} \tag{4a}$$

as

$$[\mathbf{Q} + p(\mathbf{R} + \mathbf{R}^{\mathrm{T}}) + p^2 \mathbf{T}]\mathbf{a} = \mathbf{0}. \tag{4b}$$

The six eigenvalues p_α appear only in complex conjugate pairs and can be written as p_α and $p_{\alpha+3} = \bar{p}_\alpha$ with $\alpha = 1, 2, 3$ (Eshelby *et al.*, 1953). Here and in the following, an overbar

denotes the complex conjugates. The displacement **u** and traction vector **t** on a radial line making an angle θ to the x_1 axis can be expressed as a linear combination of eigenvectors $\mathbf{a}_\alpha$ as

$$\mathbf{u} = \sum_{\alpha=1}^{3} [m_\alpha \mathbf{a}_\alpha f(Z_\alpha) + n_\alpha \bar{\mathbf{a}}_\alpha f(\bar{Z}_\alpha)]$$

$$\mathbf{t}(\theta) = \frac{1}{r} \sum_{\alpha=1}^{3} \left(m_\alpha \mathbf{b}_\alpha Z_\alpha \frac{\mathrm{d}}{\mathrm{d}Z_\alpha} f(Z_\alpha) + n_\alpha \bar{\mathbf{b}}_\alpha \bar{Z}_\alpha \frac{\mathrm{d}}{\mathrm{d}\bar{Z}_\alpha} f(\bar{Z}_\alpha) \right) \tag{5}$$

where $\mathbf{b}_\alpha$ is an associate vector directly related to the eigenvector $\mathbf{a}_\alpha$ and the matrices **Q**, **R** and **T** as

$$\mathbf{b}_\alpha = (\mathbf{R}^{\mathrm{T}} + p_\alpha \mathbf{T})\mathbf{a}_\alpha = -\frac{1}{p_\alpha}(\mathbf{Q} + p_\alpha \mathbf{R})\mathbf{a}_\alpha, \tag{6}$$

and m_α, n_α ($\alpha = 1, 2, 3$) are arbitrary constants which depend upon the specific boundary value problem at hand.

3. PROBLEM STATEMENT AND SOLUTION STRATEGY

Figure 1 defines the analyzed geometry. The grain boundary AB is considered to be fully decohered and the crack tip is located at the grain triple junction A. With x_1 axis aligned with the crack AB, the orientations of the other two boundaries are defined by the angles α_1 and α_2 with respect to the polar coordinate system centered at the triple point. The orientations of the three grains are specified, respectively, by the angles θ_1, θ_2 and θ_3 of the most compliant direction (shown by a shorter line in Fig. 1) with respect to the global x_1 axis for orthotropic grains. For cubic grains these angles define orientations of one of the material axes. The stress singularities at the crack tip were determined for different combinations of α_1, α_2, θ_1, θ_2 and θ_3. Since the material in all grains is identical, the elastic deformation within each grain will be governed by the eigenvalue problem in eqn (3), with eigenvectors $\mathbf{a}_\alpha$ and associates $\mathbf{b}_\alpha$ (eqn (6)). Let us further define matrices **A** and **B** as the collection of these eigenvectors as

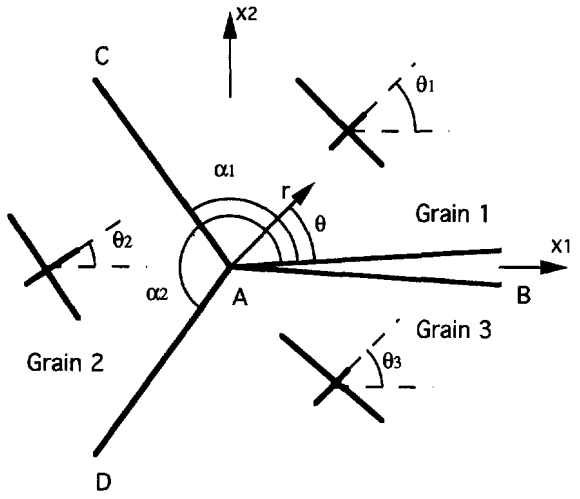

Fig. 1. Details of the geometry at a grain triple junction.

$$\mathbf{A} = [\mathbf{a}_1, \mathbf{a}_2, \mathbf{a}_3], \quad \mathbf{B} = [\mathbf{b}_1, \mathbf{b}_2, \mathbf{b}_3]. \tag{7}$$

Since the stress field is of separable form near the triple junction, the complex function $f(Z)$ in eqn (5) can be taken as

$$f(Z) = \frac{1}{\gamma+1} Z^{\gamma+1}, \tag{8}$$

where γ is a complex number. The displacements and the tractions on a radial plane can be expressed in the local coordinate system of grain "i" (denoted by the superscript) using eqns (5) and (8) as

$$\mathbf{u}^i = \frac{1}{\gamma+1}[\mathbf{A}\mathbf{Z}^i\mathbf{m}^i + \bar{\mathbf{A}}\bar{\mathbf{Z}}^i\mathbf{n}^i], \quad \mathbf{t}^i(\theta) = \frac{1}{r}[\mathbf{B}\mathbf{Z}^i\mathbf{m}^i + \bar{\mathbf{B}}\bar{\mathbf{Z}}^i\mathbf{n}^i] \tag{9}$$

where

$$\mathbf{Z}^i = \begin{pmatrix} (Z_1^i)^{\gamma+1} & 0 & 0 \\ 0 & (Z_2^i)^{\gamma+1} & 0 \\ 0 & 0 & (Z_3^i)^{\gamma+1} \end{pmatrix} \tag{10}$$

$$Z_\alpha^i = x_1^i + p_\alpha x_2^i = r(\cos\theta^i + p_\alpha \sin\theta^i), \quad i = 1,2,3$$

and $\mathbf{m}^i$ and $\mathbf{n}^i$ are two 3×1 vectors with unknown components m_α^i and n_α^i, which in turn are to be determined for each grain from the boundary conditions.

The boundary value problem associated with the configuration in Fig. 1 is defined by the continuity of displacements $\mathbf{u}$ and tractions $\mathbf{t}$ at the grain boundaries AC and AD and by the traction-free condition on both faces of the crack AB. This leads to a system of 18 equations in terms of the unknown components m_α^i and n_α^i. Using the identities (Ting, 1986)

$$\mathbf{A}^T\mathbf{B} + \mathbf{B}^T\mathbf{A} = \mathrm{I}, \quad \mathbf{A}^T\bar{\mathbf{B}} + \mathbf{B}^T\bar{\mathbf{A}} = \mathbf{0}, \quad \bar{\mathbf{A}}^T\bar{\mathbf{B}} + \bar{\mathbf{B}}^T\bar{\mathbf{A}} = \mathrm{I}, \quad \bar{\mathbf{B}}^T\mathbf{A} + \bar{\mathbf{A}}^T\mathbf{B} = \mathbf{0} \tag{11}$$

the system can be reduced to six equations with six unknowns (12).

$$\mathbf{D}\mathbf{m}^2 + \bar{\mathbf{D}}\mathbf{n}^2 = \mathbf{0}, \quad \mathbf{E}\mathbf{m}^2 + \bar{\mathbf{E}}\mathbf{n}^2 = \mathbf{0} \tag{12}$$

$\mathbf{D}$ and $\mathbf{E}$ are 3×3 matrices defined by

$$\begin{aligned} \mathbf{D} &= \omega^{10}[\mathrm{Re}\,(\mathbf{B}\mathbf{X}^1\mathbf{B}^T)\omega^{21}\mathbf{A} + \mathrm{Re}\,(\mathbf{B}\mathbf{X}^1\mathbf{A}^T)\omega^{21}\mathbf{B}]\mathbf{Z}_{12}^2 \\ \mathbf{E} &= \omega^{30}[\mathrm{Re}\,(\mathbf{B}\mathbf{X}^3\mathbf{B}^T)\omega^{23}\mathbf{A} + \mathrm{Re}\,(\mathbf{B}\mathbf{X}^3\mathbf{A}^T)\omega^{23}\mathbf{B}]\mathbf{Z}_{32}^2 \end{aligned} \tag{13}$$

where the matrices of rotation ω^{ij} relate the local coordinate system in grains i and j, and the matrices $\mathbf{X}^i$ and $\mathbf{Z}_{ji}^i$ $(i,j = 1, 2, 3)$ are diagonal with elements

$$X_{\alpha\alpha}^i = \left(\frac{\cos\theta^{ij} + p_\alpha \sin\theta^{ij}}{\cos\theta^{ik} + p_\alpha \sin\theta^{ik}}\right)^{\gamma+1}, \tag{14}$$

and

$$Z_{ji}^i = (\cos\theta^{ij} + p_\alpha \sin\theta^{ij})^{\gamma+1}. \tag{15}$$

Here θ^{ij} and θ^{ik} refer to the position of the grain boundaries that grain i makes with grains

j and k, respectively. Further, both angles are measured in the local coordinate system of grain i with grains j and k located anti-clockwise and clockwise to grain i, respectively.

Since **D** and **E** are nonsingular, the system (12) can be further simplified to

$$(\mathbf{E}\mathbf{D}^{-1} - \overline{\mathbf{E}\mathbf{D}}^{-1})\mathbf{m}^2 = \mathbf{0}. \tag{16}$$

For nontrivial solutions, the 3×3 determinant of (16) has to be zero. This defines the eigenvalue problem in the form

$$\det [\mathrm{Im}\,(\mathbf{E}\mathbf{D}^{-1})] = 0. \tag{17}$$

The roots γ of eqn (17) have been found numerically. Some of the results were confirmed using a finite element iterative method similar to the one described by Barsoum (1988) and Barsoum and Chen (1991). After six iterations the analytically found singularities were recovered up to the third decimal place. In all investigated cases no complex singularities were found.

4. RESULTS AND DISCUSSION

Consider first the grains to be transversely orthotropic. When the x_1–x_2 coordinate system is aligned with the material axes, the equations of elasticity for the plane problem are prescribed in terms of four independent elastic constants c_{11}, c_{22}, c_{12} and c_{44} as

$$\sigma_{11} = c_{11}\varepsilon_{11} + c_{12}\varepsilon_{22}, \quad \sigma_{22} = c_{12}\varepsilon_{11} + c_{22}\varepsilon_{22}, \quad \sigma_{12} = 2c_{44}\varepsilon_{12}. \tag{18}$$

As shown by Suo (1990), for a simply connected domain and for traction prescribed boundary conditions, the stress σ_{ij} and hence the singularity γ depend only on two non-dimensional parameters

$$\lambda = \frac{c_{22}}{c_{11}}, \quad \rho = \frac{1}{c_{44}} \frac{c_{11}c_{22} - c_{12}^2 - 2c_{12}c_{44}}{2\sqrt{(c_{11}c_{22})}} \tag{19}$$

For the strain energy to be bounded, ρ takes values higher than -1 whereas λ is always greater than 1. A value of $\lambda = 1$ corresponds to the transversely cubic case, whereas for $\lambda = \rho = 1$ the material degenerates into a transversely isotropic one. Most engineering materials have λ values between 1 and 5 and ρ values between 0 and 5. Several examples are listed in Table 1. In the following, unless specified, all calculations have been made with $\lambda = 2$ and $\rho = 0.52$.

Studies of stress concentration at triple grain junctions induced by the elastic anisotropy of the grains (Tvergaard and Hutchinson, 1988; Picu and Gupta, 1995) have shown that symmetric configurations always lead to an enhanced concentration effect. Hence, here only symmetric configurations are studied.

Table 1. Non-dimensional parameters λ, ρ and Q, R for several idealized transversely orthotropic and cubic materials. The elastic constants of the listed materials were taken from Simmons and Wang (1985)

Material	Q	R	Material	λ	ρ
CaO	0.54	1.25	apatite	1.19	0.5
ZrC	3.57	0.78	calcite	1.72	0.65
TiC	1.54	0.92	sapphire	1.08	1.36
Ge	1.39	1.41	TiB_2	1.57	0.28
Si	1.27	1.39	$BaTiO_3$	1.05	0.95

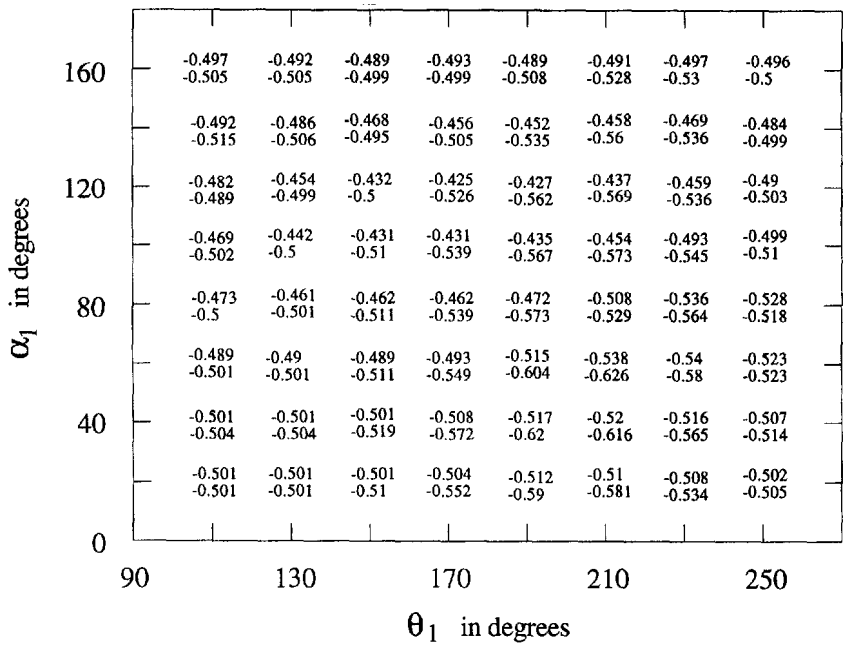

Fig. 2. Variation of the singularity exponent γ in the α_1–θ_1 plane for symmetric configurations defined by $\alpha_2 = 360° - \alpha_1$, $\theta_1 = -\theta_3$ and $\theta_2 = 90°$. In one pair of data the value above and the one below correspond to mode I and mode II loading, respectively. All points along the border of the diagram correspond to configurations with a singularity of $-\frac{1}{2}$ for both loading modes. The grains are made from a transversely orthotropic material with $\lambda = 2$ and $\rho = 0.52$.

Let us consider first the case when the grain angles α_1 and α_2 are varied simultaneously such that $\alpha_2 = 360° - \alpha_1$, $\theta_1 = -\theta_3$ and $\theta_2 = 90°$. Figure 2 shows the variation of the singularity at the crack tip for the whole range of α_1 and θ_1 and for both mode I and mode II loading. The singularities corresponding to the symmetric and antisymmetric fields are different.

A similar effect was reported by Bazant and Estenssoro (1979) when analyzing 3D stress concentrations of a crack meeting a free surface, and in some other 3D problems analyzed by Barsoum and Chen (1991). In two dimensions, a similar *fixed* mode was found by He and Hutchinson (1989) at the tip of an oblique crack terminating at an interface between two isotropic materials, whereas the variation of the singularity exponents with the material and geometrical parameters for the same problem has been fully investigated by Wang and Chen (1994). Since in their case the problem is not geometrically symmetric, the field related to the strongest singularity exponent represents a fixed *mixed* mode, independent of the remote loading combination acting on the body. In the present case, due to the assumed geometrical symmetry, the two eigenvalues found in the $(-1, 0)$ domain correspond to fields which can be taken as symmetric and antisymmetric with respect to the crack line. Since the strongest singularity dominates in a small region close to the tip, a fixed mode governs the crack propagation. However, for non-symmetric triple junction configurations, a fixed *mixed* mode is expected to exist at the crack tip.

Even for a simple uniaxial loading applied on a polycrystal, a unique loading mode on an internal microcrack cannot be expected. As shown in Fig. 2, for almost all configurations at least one of the loading modes is related to a super-singularity such that, under mixed mode conditions, the crack is expected to propagate unstably away from the triple junction. The effect of the anisotropy is shown to be in general a shielding of mode I cracks and an enhancement of the singularity for mode II cracks. However, there are configurations ($\alpha_1 < 90°$, $\theta_1 > 180°$) for which both loading modes lead to a super-singularity.

Figure 3 shows the similar γ variation for another set of symmetric configurations defined by ($\alpha_2 = 360° - \alpha_1$, $\theta_1 = -\theta_3$ and $\theta_2 = 0°$). Configurations with $\alpha_1 > 90°$ and $90° < \theta_1 < 180°$ lead to a different effect upon the two loading modes. Mode I corresponds

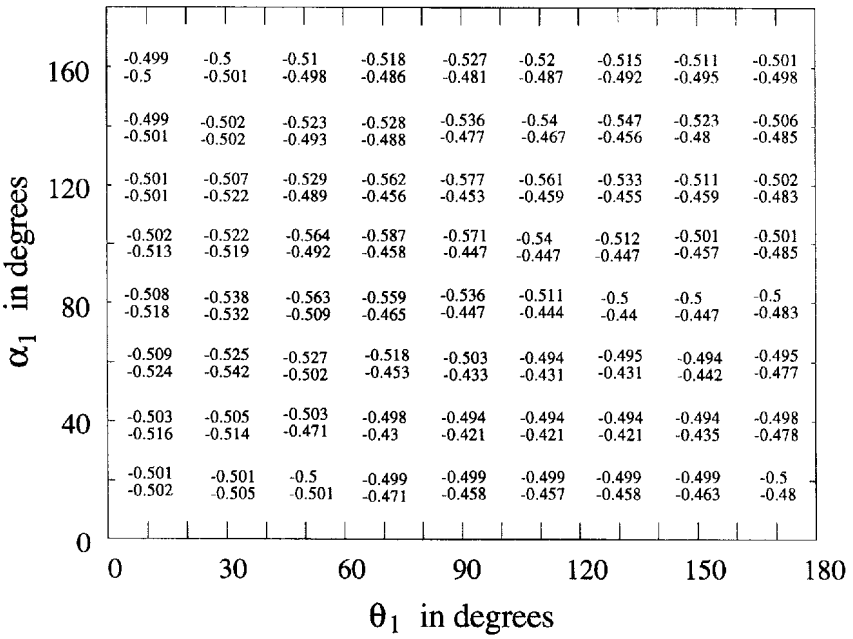

Fig. 3. Variation of the singularity exponent γ in the α_1–θ_1 plane for symmetric configurations defined by $\alpha_2 = 360^\circ - \alpha_1$, $\theta_1 = -\theta_3$ and $\theta_2 = 0^\circ$. In one pair of data the value above and the one below correspond to mode I and mode II loading, respectively. All points along the border of the diagram correspond to configurations with a singularity of $-\frac{1}{2}$ for both loading modes. The grains are made from a transversely orthotropic material with $\lambda = 2$ and $\rho = 0.52$.

to super-singular fields while mode II is shielded. This is an opposite situation with respect to the one in Fig. 2 for the same region of the diagram. However, for angles $\alpha_1 < 80^\circ$ and $\theta_1 < 60^\circ$ both modes are super-singular and the crack propagates unstably for any loading mode. If $\alpha_1 < 80^\circ$ and $\theta_1 > 100^\circ$ one finds the opposite situation when both modes correspond to singularities weaker than $-\frac{1}{2}$ and the crack tip is shielded. In this case, in the absence of dynamic effects, an interface crack which reaches the triple junction is arrested and more strain energy has to build up in the material for it to further propagate.

For all investigated geometries, the highest effect of the anisotropy is obtained in the symmetric case defined by $\alpha_1 = 120^\circ$, $\alpha_2 = 240^\circ$, $\theta_1 = \theta_3 = 0^\circ$ and $\theta_2 = 90^\circ$ ($\gamma = -0.425$ for mode I and $\gamma = -0.545$ for mode II loading). As mentioned before, mode II leads to a super-singularity while mode I corresponds to a singularity weaker than $-\frac{1}{2}$. Figure 4 shows the stress singularities for both modes for various orthotropic crystals and for the most singular configuration obtained above. The effect of the anisotropy increases with increasing λ while the dependence upon ρ is weaker. For $\lambda = 1$, the material becomes transversely cubic and, given the geometrical configuration at hand, the three grains become identical such that the crack is embedded in an homogeneous material. The standard $-\frac{1}{2}$ singularity is recovered.

The effect of the anisotropy on the crack tip singularity has been investigated for several non-symmetric configurations. The variation of γ for the case defined by ($\alpha_1 = 120^\circ$, $\alpha_2 = 240^\circ$, $\theta_1 = 0^\circ$ and $\theta_2 = 90^\circ$) and by ($\alpha_1 = 120^\circ$, $\alpha_2 = 240^\circ$, $\theta_1 = 0^\circ$ and $\theta_3 = 0^\circ$) and for the whole range of variation of θ_3 and θ_2, respectively, has been analyzed. In both cases the strongest effect of the anisotropy corresponds to the symmetric configuration, a result consistent with the one reported in Picu and Gupta (1995).

Let us consider next the transversely cubic grains with their 1–2 axes aligned with the x_1–x_2 coordinate system. For traction-prescribed boundary conditions the plane deformation is characterized by two non-dimensional parameters Q and R defined by

$$Q = \frac{c_{44}}{c_{12}}, \quad R = \frac{c_{12} + 2c_{44}}{c_{11}}. \tag{20}$$

For isotropic materials R assumes a value of unity. Table 1 shows the values of Q and R for

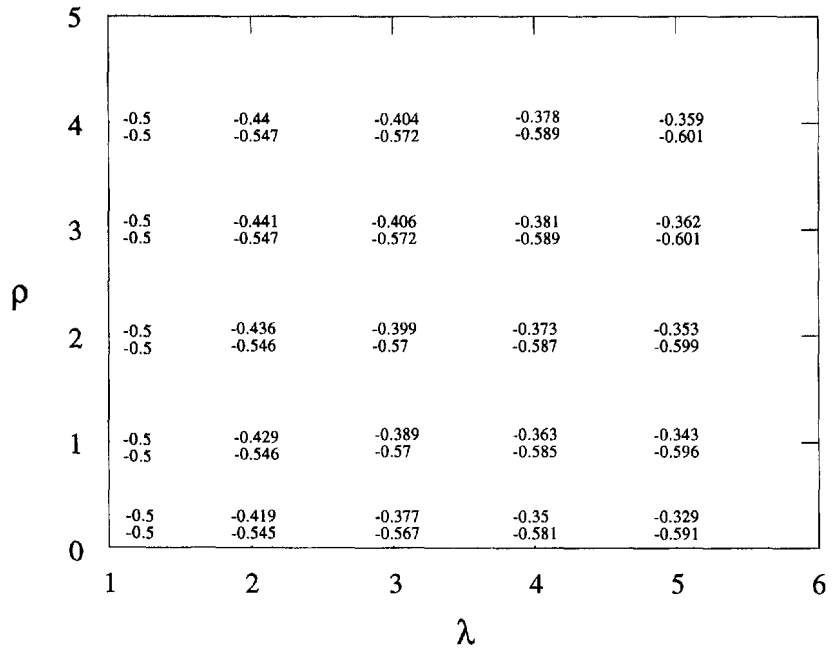

Fig. 4. Values of the singularity exponent γ for various polycrystals with orthotropic grains characterized by two material parameters λ and ρ. The calculations have been performed for the configuration defined by $\alpha_1 = 120°$, $\alpha_2 = 240°$, $\theta_1 = \theta_3 = 0°$ and $\theta_2 = 90°$.

some representative ceramics and minerals. Similar to the orthotropic case, only symmetric configurations have been investigated.

Figure 5 shows the variation of the singularity γ with α_1 and θ_1 for the case defined by $\alpha_2 = 360° - \alpha_1$, $\theta_1 = -\theta_3$ and $\theta_2 = 0°$. The results are obtained for the specific case of TiC ($Q = 1.54$, $R = 0.92$). Singularities corresponding to the symmetric and antisymmetric fields are shown. For almost the full range of variation of α_1 and θ_1 at least one mode leads

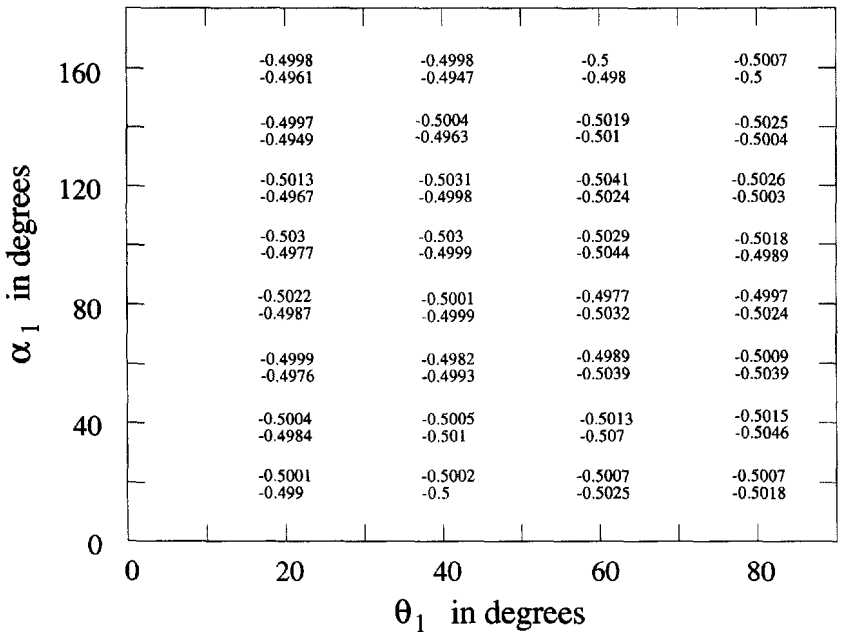

Fig. 5. Variation of the singularity exponent γ in the α_1–θ_1 plane for symmetric configurations defined by $\alpha_2 = 360° - \alpha_1$, $\theta_1 = -\theta_3$ and $\theta_2 = 0°$. All points along the border of the diagram correspond to configurations with a singularity of $-\frac{1}{2}$ for both loading modes. The grains are made from TiC with $Q = 1.54$ and $R = 0.92$.

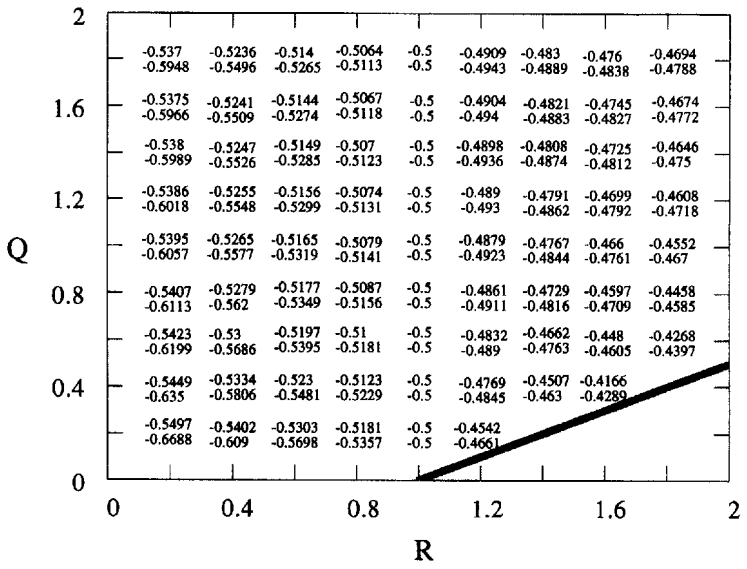

Fig. 6. Variation of the singularity exponent γ with the two non-dimensional material parameters Q and R for the symmetric configuration of cubic grains defined by $\alpha_1 = 120°$, $\alpha_2 = 240°$, $\theta_1 = -\theta_3 = 60°$ and $\theta_2 = 0°$. The bold line represents a border below which real materials cannot exist. The singularities for both mode I (above) and mode II (below) loading are shown.

to a super-singularity. However, for some combinations of the two parameters α_1 and θ_1 both modes correspond to singularities weaker than $-\frac{1}{2}$. Compared with the similar map for orthotropic materials, the zone of crack tip shielding is smaller.

The low level of anisotropy of TiC leads to a rather small effect on the crack tip singularity. However, the effect is expected to become more significant when increasing Q and R. To investigate this, two particular geometrical configurations were considered. First, for the symmetric configuration defined by $\alpha_1 = 120°$, $\theta_1 = 60°$ and $\theta_2 = 0°$, the parameters R and Q have been varied and the change in γ is illustrated in Fig. 6. The bold line represents a border below which real materials cannot exist since the positive definiteness of the strain energy density is not satisfied. The line $R = 1$ which corresponds to isotropic materials defines two regions in the map. For $R > 1$ the investigated geometry leads to a decrease in the crack tip singularity. In materials with $R < 1$, such a configuration leads to super-singularities for both loading modes. The effect is stronger for mode II loading. The singularity γ decreases with increasing R and Q in the region $R < 1$, the dependence on Q being weaker. For $R > 1$ the singularity increases with increasing Q.

Figure 7 shows a similar map for the symmetric configuration defined by $\alpha_1 = 140°$, $\theta_1 = 20°$ and $\theta_2 = 0°$. Here, for $R > 1$ both loading modes lead to super-singular fields while for $R < 1$ singularities weaker than $-\frac{1}{2}$ are obtained. Unlike the previous case, a stronger effect is observed under mode I loading, in the shielding domain $R < 1$. The highest singularities γ of the map are predicted for materials located close to the bold line.

5. CONCLUSIONS

The effect of the level of anisotropy and the relative orientation of the principal material axes on the crack-tip stress-field singularity for a crack lying along a grain boundary in a single-phase polycrystalline material, and impinging on a triple grain junction has been investigated. Both cubic and orthotropic grains and only symmetric configurations have been considered. A fixed mode at the crack tip, similar with the one found for a crack impinging at an oblique angle into an interface between two isotropic materials was found. Due to the assumed symmetric configuration of the triple junction, here there is no mode mixity at the crack tip and each eigenvalue corresponds either to mode I or mode II loading.

Some configurations lead to super-singularities which, in the absence of dynamic or plastic effects implies an unstable propagation of the crack away from the triple junction

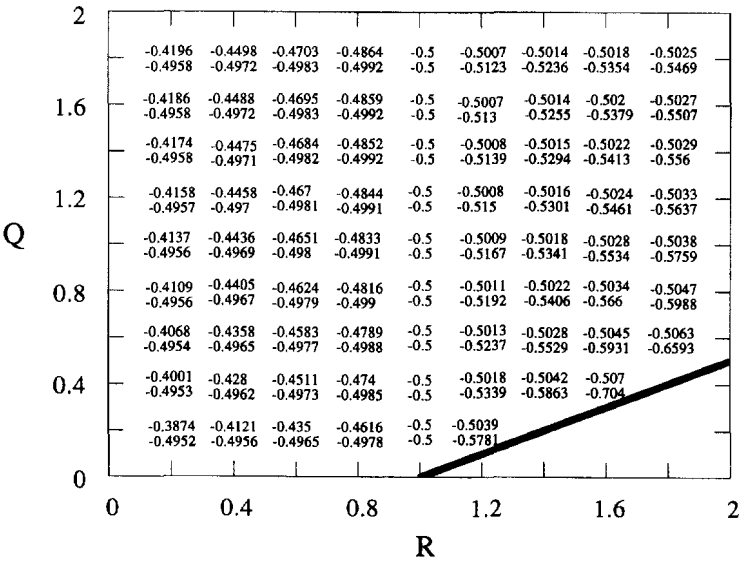

Fig. 7. Variation of the singularity exponent γ with the two non-dimensional material parameters Q and R for the symmetric configuration of cubic grains defined by $\alpha_1 = 140°$, $\alpha_2 = 220°$, $\theta_1 = -\theta_3 = 20°$ and $\theta_2 = 0°$. The bold line represents a border below which real materials cannot exist. The singularities for both mode I (above) and mode II (below) loading are shown.

while some others lead to singularities weaker than $-\frac{1}{2}$. This second effect is similar to the shielding of the crack tip such that more energy will be required to be stored in the material in order to propagate the crack. In most cases while one loading mode leads to a singularity weaker than $-\frac{1}{2}$, the other mode may be associated with a super-singularity. In compression, if mode I opening is inhibited, the behavior depends only upon the mode II singularity and, for certain configurations, an important shielding effect may be obtained. Similar to the case of an interface crack between orthotropic or cubic materials where the out-of-plane and the in-plane deformation modes are decoupled, here only real singularities were found.

Acknowledgments—This work was supported by the U.S. Office of Naval Research, under grant no. N00014-92-J-1247.

REFERENCES

Barsoum, R. S. (1988). Theoretical basis of the finite element iterative method for the eigenvalue problem in stationary cracks. *Int. J. Numer. Meth. Eng.* **26,** 531–539.

Barsoum, R. S. and Chen, T. K. (1991). Three-dimensional surface singularity of an interface crack. *Int. J. Fract.* **50,** 221–237.

Bazant, Z. P. and Estenssoro, L. F. (1979). Surface singularity and crack propagation. *Int. J. Sol. Struct.* **15,** 405–426.

Chen, Y. Z. and Hasebe, N. (1993). Singularity eigenvalue analysis of a crack along a wedge-shaped interface. *J. Appl. Mech.* **60,** 781–782.

Comninou, M. (1977a). The interface crack. *J. Appl. Mech.* **44,** 631–636.

Comninou, M. (1977b). The interface crack in a shear field. *J. Appl. Mech.* **45,** 287–290.

Eshelby, J. D., Read, W. T. and Shockley, W. (1953). Anisotropic elasticity with application to dislocation theory. *Acta Metall.* **1,** 251–259.

Evans, A. G. (1978). Microfracture from thermal expansion anisotropy—single phase systems. *Acta Metall.* **26,** 1845–1853.

Fu, Y. and Evans, A. G. (1985). Some effects of microcracks on the mechanical properties of brittle solids—stress–strain relations. *Acta Metall.* **33,** 1515–1523.

He, M. Y. and Hutchinson, J. W. (1989). Crack deflection at an interface between dissimilar elastic materials. *Int. J. Sol. Struct.* **25,** 1053–1067.

Lekhnitskii, S. G. (1963). *Theory of Elasticity of an Anisotropic Body*. Holden-Day, San Francisco.

Qu, J. and Bassani, J. L. (1989). Cracks on bimaterial and bicrystal interfaces. *J. Mech. Phys. Sol.* **37,** 417–433.

Picu, C. R. and Gupta, V. (1995). Singularities at grain triple junctions in two dimensional polycrystals with cubic and orthotropic grains. *J. Appl. Mech.* (in press).

Simmons, G. and Wang, H. (1985). *Single Crystal Elastic Constants and Calculated Aggregate Properties: a Handbook*. The MIT Press, Cambridge. Massachusetts.

Suo, Z. (1990). Delamination specimens for orthotropic materials. *J. Appl. Mech.* **57,** 627–634.

Ting, T. C. T. (1986). Explicit solutions and invariance of the singularities at an interface crack in anisotropic composites. *Int. J. Sol. Struct.* **22,** 965–983.

Tvergaard, V. and Hutchinson, J. W. (1988). Microcracking in ceramics induced by thermal expansion or elastic anisotropy. *J. Amer. Ceram. Soc.* **71,** 157–166.

Wang, W. C. and Chen, J. T. (1994). Singularities of an arbitrarily inclined semi-infinite crack meeting a bimaterial interface. *Eng. Fract. Mech.* **49,** 671–680.

Williams, W. L. (1959). The stress around a fault or crack in dissimilar media. *Bull. Seism. Soc. Amer.* **49,** 199–204.